Kertesz Szabolcs (Orcid ID: 0000-0001-9760-3008)

Evaluation of VSEP module-integrated 3D printed spacers for enhanced wastewater ultrafiltration

Szabolcs Kertész*
Department of Biosystems Engineering, Faculty of Engineering, University of Szeged, Szeged H-6725, Hungary
*kertesz@mk.u-szeged.hu

Abstract

The article evaluates the effectiveness of two new designed module-integrated 3D printed spacers in enhancing wastewater ultrafiltration efficiencies using Vibratory Shear Enhanced Processing (VSEP). The study investigates the star-shaped spacer filled module channel (Star spacer) and the column-shaped herringbone spacer filled module channel with the same position as the flow direction (Column spacer) and with the opposite position as the flow direction (Rev column spacer). It compares the VSEP module-integrated spacers with membrane module vibration (Module vibration) and empty membrane module channel (Control) configurations. The results show that the module integration of the 3D printed spacers can greatly improve the specific, average and constant permeate fluxes and can contribute to reducing the total, reversible and irreversible resistance values and specific energy consumption of the ultrafiltration membrane separation experiments. Overall, this study provides valuable insights into improving the performance of wastewater ultrafiltration systems and fouling mitigation through the module-integration of 3D printed spacers and membrane module vibration.

Keywords: 3D Printed Spacers; VSEP; Ultrafiltration; Dairy wastewater; Membrane fouling.

Highlights:

• VSEP ultrafiltration module-integrated 3D printed spacers were successfully fabricated and evaluated for improved wastewater treatment.

• Two spacer designs, a star-shaped and a column-shaped herringbone, were compared to an empty membrane module channel with and without vibration.

• Two configurations of the column-shaped spacer, in the same and reversed flow direction, were tested.

• Specific energy consumption was calculated and compared for all configurations.

• Significant improvements in ultrafiltration performance were observed with the use of spacers compared to an empty module channel, including enhanced permeate fluxes and reductions in both total and reversible, as well as irreversible, resistance.

INTRODUCTION

The dairy industry represents a significant contributor to water pollution (Labbé et al., 2017) due to the substantial concentration of organic matter that results in high chemical oxygen demand (COD) (Andrade et al., 2014). If not treated or disposed of appropriately, dairy wastewater poses a substantial environmental challenge (Bortoluzzi et al., 2017). Several technologies have been employed to treat dairy wastewater (Kumar et al., 2015; Bhuvaneshwari et al., 2022). Among these, membrane technology stands out as one of the most promising due to its high efficiency in the treatment process (Fritzmann et al., 2014; Yanar et al., 2018). In addition to its established use in the food industry for the treatment of food products, by-products, and wastewater (Reig et al., 2021), membrane technology has gained widespread adoption in the treatment of dairy wastewater (Galvão, 2018). This technology offers many

advantages, including ease of operation, relatively lower operational costs compared to conventional methods, and no need for additional chemicals (Park et al., 2021). Furthermore, membrane technology is compatible with other processing methods, such as chemical, physical, or biological procedures (Nqombolo et al., 2018).

However, the biggest drawback of using membranes is their susceptibility to fouling during filtration (Baitalow et al., 2021; Sreedhar et al., 2018). This phenomenon occurs due to the formation of a polarization layer on the membrane surface (Guo et al., 2012), which results in the deposition of various components on the membrane surface and in the pores (Aslam et al., 2022), leading to adsorption or blockage and a significant reduction in their efficiency (Tanudjaja et al., 2022). Significant efforts have been made by scientists to mitigate or prevent the occurrence of this phenomenon, at the same time, recent technological advancements have introduced 3D printing to the field of water and wastewater treatment, revolutionizing traditional manufacturing methods (Ng et al., 2021; Thomas et al., 2019). 3D printed elements exhibit superior filtration properties in membrane separation processes (Ali et al., 2019), compared to conventional plastic spacers (Sreedhar et al., 2022), presenting a promising avenue for enhancing treatment efficiency and reducing environmental impact (Van Dang et al., 2021).

Over the past decade, there have been significant advancements in three-dimensional (3D) printing technology, including printing resolution, speed, and cost. This has led to breakthroughs in membrane fabrication for water treatment. Despite conflicting reports on the feasibility of 3D printing for membranes, successful prototypes have been fabricated due to the high degree of freedom in material and prototype design (Koo et al., 2021). Khalil et al. (2021) have reported that in thermal desalination, 3D printed components are utilized to improve water evaporation and energy harvesting through novel designs and materials. In the case of membrane-based desalination, 3D printing offers the potential for the production of customized membrane modules and other components with improved fouling resistance and productivity, by employing tailored materials and geometries. Al-Shimmery et al. (2019) reported on the fabrication of 3D printed composite membranes by depositing a thin polyethersulfone (PES) selective layer onto 3D printed flat and wavy structured substrates with ABS-like characteristics. The results of the study indicate that the use of 3D printed corrugated composite membranes can significantly enhance permeation and cleaning performance, particularly in terms of reducing fouling build-up.

In a study by Tsai et al. (2019), 3D printed turbulence promoters were tested in cross-flow microfiltration, showing potential for reducing fouling and enhancing filtration. Operating conditions and fluid velocity were examined using computer fluid design (CFD). Gáspár and Neczpál (2020) reports on the development of turbulence promoter geometries using fused deposition modeling (FDM) 3D printing technology, which are effective in intensifying permeate flux and retention in membrane filtration, with the same geometry as existing metallic versions. The experiments demonstrated that 3D printed static mixers are as effective as metallic versions, but with a slightly higher pressure drop, which can be reduced by using a smaller nozzle or smoothing the surface. PETG is recommended due to its higher operating temperature and better water-resistant properties.

One potential approach to mitigate membrane fouling involves employing module vibration through the utilization of Vibratory Shear Enhanced Processing (VSEP), which can lower operational costs above a critical pressure value (Szerencsés et al., 2021). VSEP technology has been successfully used in several studies to treat high-organic solutions, such as dairy wastewaters (Akoum et al., 2004; Frappart et al., 2006). These studies used the entire range of membranes available (MF, UF, NF, and RO) and demonstrated significant advantages of the VSEP system over traditional membrane processes. Shi and Benjamin (2009) demonstrated that fouling of reverse osmosis (RO) membranes can be alleviated by inducing high shear rates at the membrane surface through torsional vibration of flat sheet membranes. They conducted experiments using a vibratory shear enhanced filtration process (VSEP) system to treat simulated brackish water source and brine. The results revealed that vibration significantly reduced membrane fouling.

The objective of this study was to investigate the performance of two different module-integrated 3D printed spacers, fabricated through FDM technique, for membrane fouling mitigation in a VSEP system with three different configurations and compare them with the control empty membrane module channel configurations. Through experimental testing and comparative analysis, the study aims to provide insights into the performance of the two new designed spacers and their potential for improving ultrafiltration membrane efficiency.

MATERIALS AND METHODS

Preparation of Model Wastewater

A model dairy wastewater was prepared by combining tap water with 5 g/L of skimmed milk powder (Tutti Food Industry Ltd., Rábapatona, Hungary) and Cl80 anionic detergent at a concentration of 0.5 g/L (Hungaro Chemicals, Nagycserkesz, Hungary). The mixture was homogenized for 30 minutes using a Scilogex 4-prong metal head mixer at 450 RPM. The temperature of the wastewater was maintained at a controllable room temperature of 25±1°C during membrane filtration experiments using a home-made 10-liter double-walled feed tank. The feed tank was equipped with a submerged snake cooler, which was filled with circulating cooling liquid from a 300L buffering tank that was cooled with an air conditioning system (Galletti S.p.A., Italy).

Membrane and membrane separation equipment

This study investigates the performance of a 50 kDa poliethersulfone (PES) ultrafiltration membrane (Microdyn-Nadir, USA) with an effective filtration area of ~0.05 m2 at 25±1°C, 0.8 MPa transmembrane pressure (TMP), and recirculation cross-flow rate (q_{VREC}) of 4 GPM (~15.142 LPM). A laboratory-scale Vibratory Shear Enhanced Processing (VSEP) membrane separation equipment (New Logic Research Inc., USA) was employed for the study (Figure 1), which utilizes a unique feature of vibrating the membrane module at a specific frequency. The module vibration experiments were carried out with a vibration amplitude of 2.54 cm, which is the maximum value that can be adjusted. The experiments were also performed without vibration as control. In addition, two different 3D printed spacers were designed and integrated into the module flow channel between the membrane active filtration side and the module bottom. These spacers served as binding elements, supporting the membrane during filtration, maintaining a constant distance between the membrane surface and the module, and increasing local turbulence at the membrane surface to obtain reliable and consistent results. All experiments were conducted in triplicate.

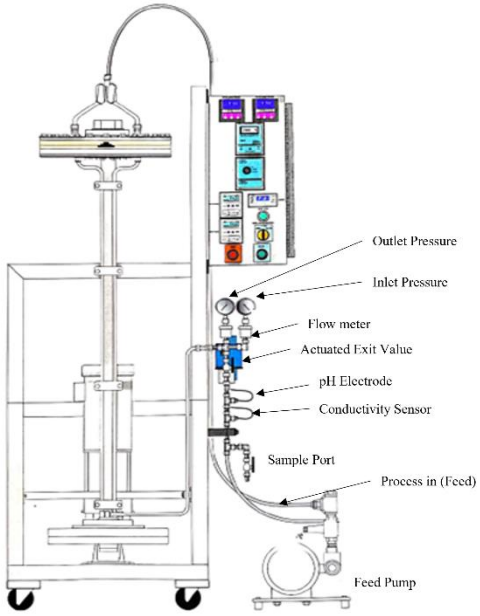

Figure 1. Exploded view of the equipment (right) (Source: VSEP L-mode Unit Operation Manual)

The 10-liter feed tank was filled with a pre-homogenized model dairy wastewater as a feed, which was pumped towards the module using a feed pump. The cross-flow technology facilitated the separation of the model into wastewater filtrate, as a permeate and concentrated, as a retentate due to the TMP. The concentrate was recirculated back to the feed tank while the filtrate was directed through a separate pipe to the collection vessel for permeate volume measuring.

Analytics

During the ultrafiltration experiments, 45-45 mL of the feed wastewater, permeate, and concentrate were collected for analytical measurements to analyze turbidity, conductivity, and organic content.

Turbidity and conductivity analysis

The turbidity of the sample was determined using a HACH 2100AN turbidimeter (USA). 10 mL of the sample was filled into a special glass cuvette, and the amount of light scattering caused by suspended particles in the sample was measured in Nephelometric Turbidity Units (NTU). The instrument was calibrated with a standard solution before measurement. Conductivity was measured using a Consort BVBA C5010 conductivity meter (Belgium). The instrument was calibrated using distilled water before measuring the conductivity of the samples, which were analyzed in a minimum volume of 10 mL.

Organic matter analysis

Chemical oxygen demand (COD) was determined using the standard method outlined in American Public Health Association (APHA) Standard Method 5220. Each 1 mL of the sample was acidified with sulfuric acid and then mixed with a solution containing potassium dichromate and mercury sulfate in a prepared test tube. Then it was placed in a digester block (ECO 8) heated to 150°C for 120 minutes to digest the organic matter. The resulting solution was cooled and measured with a spectrophotometer (Lovibond, Belgium).

3D Printed Spacers

3D printed spacers were produced using fused deposition modeling (FDM) technology with a polylactic acid (PLA) composite filament. The spacers were printed at a layer thickness of 0.2 mm, 100% filling density, and a cubic filling pattern were used for printing at a temperature of 210°C with a bed temperature of 60°C. Two fiber-reinforced fixings were placed at the point of contact between the spacer and the module to withstand the pressure of the 3D printed fibers next to the flow of the inlet and outlet of the module. Autodesk Fusion 360 and Ultimaker Cura (5.0.0.) software were used to design the spacers, which were printed using a Creality CR-10S Pro V2 3D printer (China). The module-integrated spacer with the connecting fixings was placed in the VSEP module from the direction of the inflowing sample next to the membrane (Figure 3). The height and width of the spacers were set to 3 mm and 257 mm, respectively, to fit the internal dimensions of the module perfectly. Two spacers with three configurations were tested: a star-shaped spacer filled module channel (Figure 2-A) and a column-shaped herringbone spacer with the same (Figure 2-B1) and opposite position (Figure 2-B2) as the flow direction. The star-shaped spacer had 2 x 44 pieces with a node height of 3 mm, while the column spacers had 2 x 42 pieces with a node height of 2 mm plus a 1 mm bottom layer and an outer diameter of 257 mm and an inner diameter of 100 mm. These module-integrated spacer configurations were compared with the empty membrane module channel configurations, including control without vibration and module vibration cases.

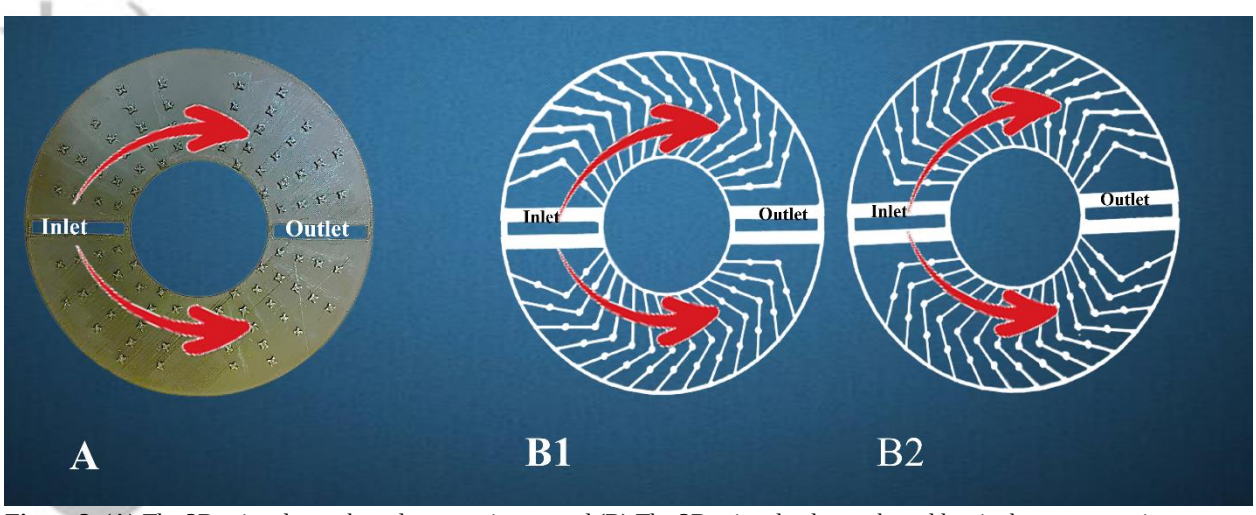

Figure 2. (A) The 3D printed star-shaped spacer picture, and (B) The 3D printed column-shaped herringbone spacer pictures (B1) in the same position as the flow direction and (B2) in the opposite position as the flow direction.

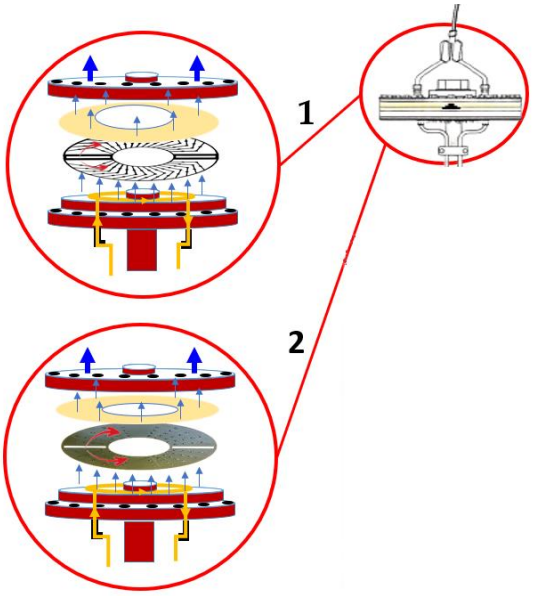

Figure 3. Visual representation delineating the precise spatial arrangement of the 3D spacers within the module.

Membrane Separation Operations: Key Characteristics and Indicators

In general, membrane filtration operations are commonly characterized by the permeate flux, which measures the mass or volume of filtrate passing through a unit area of membrane in a given time. This flux is also known as mass or volume flow density and is defined by equation (1):

$$J = \frac{V}{t \cdot A} \text{ (LMH: L/(}m^2 \cdot \text{h))} \quad (1)$$

Where (J) is the permeate flux of the tested wastewater (LMH), (V) is the volume of the permeate, (t) is the filtration time (s), and (A) is the active surface of the membrane (m^2).

The efficiency of membrane filtration was evaluated by measuring the permeate fluxes and comparing them to the corresponding conversions. Filtrate flux, a crucial parameter, provides information about the filtration speed during wastewater treatment.

The objective is to generate the maximum amount of filtrate in the shortest time possible. However, the total efficiency also depends on the energy investment, quality of the permeate, retention, and degree of fouling.

Specific flux can be calculated by TMP with the following equation (2):

$$J_{SP} = \frac{J}{TMP} \text{ (LMH/bar)} \quad (2)$$

Where (J_{SP}) is specific permeate flux (LMH), Transmembrane pressure (Pa).

To determine the flux, the permeate was collected in a measuring cylinder for a specified period, and the volume of the filtrate was recorded. The flux values were determined using equation (3):

$$J_p = \frac{TMP}{\eta \cdot (R_M + R_{IRR} + R_{REV})} \text{ (LMH)} \quad (3)$$

Where (J_p) is the permeate flux (LMH: L/(m^2·h)), (η) is the dynamic viscosity of the model wastewater at 25°C (Pas), (R_M) is the membrane resistance of the pristine membrane (1/m), (R_{IRR}) is the irreversible resistance (1/m), and (R_{REV}) is the reversible resistance (1/m).

The membrane rejection, which determines the quality of the permeate, is also known as retention and is quantified by equation (4). The chemical oxygen demand (COD, mg/L), which generally indicates the amount of retention of organic matter (%), was used as an indicator to quantify the selectivity of the membrane. Furthermore, the retention of turbidity and conductivity was also measured using the same equation, with the measured turbidity and conductivity values instead of concentrations.

$$R = \left(1 - \frac{C_P}{C_F}\right) \cdot 100 \text{ (\%)} \quad (4)$$

Where (R) is the retention value (%), (c_P) is the concentration of the permeate (mg/L), and (c_F) is the concentration of the feed (mg/L).

A detailed examination of the membrane separation resistances can provide information on the degree of fouling or the membranes' tendencies and type of fouling. Based on the resistance in series model, the permeate flux is inversely proportional to the value of the total resistance. This is closely related to the membrane's lifetime, fouling, and usability. The total resistance value, equation (5), can be determined from the sum of the different resistance values of the pristine, clean, new membrane resistance equation (6), irreversible resistance equation (7), and reversible resistance equation (8). Irreversible resistance comes from membrane pore blockages that cannot be removed by simple surface cleaning.

$$R_T = R_M + R_{IRR} + R_{REV} \quad (1/\mathrm{m}) \tag{5}$$

$$R_M = \frac{TMP}{J_{W1} \cdot \eta_W} \quad (1/\mathrm{m}) \tag{6}$$

$$R_{IRR} = \frac{TMP}{J_{W2} \cdot \eta_W} - R_M \quad (1/\mathrm{m}) \tag{7}$$

$$R_{REV} = \frac{TMP}{J_C \cdot \eta_{WW}} - R_M - R_{IRR} \quad (1/\mathrm{m}) \tag{8}$$

Where (R_T) is Total resistance (1/m), (J_{W1}) is the Water flux of the pristine membrane (LMH), (J_{W2}) is the water flux of the membrane after wastewater experiment and polarization layer removing (LMH), (J_C) is the constant permeate flux (LMH), (η_w) is the dynamic viscosity of water at 25°C (Pas), and (η_{ww}) is the dynamic viscosity wastewater (ww) at 25°C (Pas).

The irreversible resistance value was determined by removing the polarization layer by simple surface cleaning with water gently flushing and then another water ultrafiltration was carried out.
In membrane separations, a concept and indicator that is also often used is the so-called volume reduction ratio (VRR), which shows how concentrated the volume of the feed is, i.e., how the volume of the feed side is proportional to the volume of the permeate measured at a given time, and it calculated by equation (9).

$$VRR = \frac{V_F}{V_F - V_P} \quad (-) \tag{9}$$

Where (VRR) is volume reduction ratio, (V_F) is the initial volume of the feed (m^3), (V_P) is the permeate volume (m^3).

The specific energy consumption (SE) can be determined with the efficiencies and the power of the feed pump and vibration motor, using the measured permeate flux and the active membrane filtration surface by equation (10).

$$SE = \frac{\eta_{FP} \cdot P_{FP} + \eta_{VM} \cdot P_{VM}}{J \cdot A} \ (\mathrm{kWh/m^3}) \tag{10}$$

Where (SE) is specific energy consumption (kWh/m^3), (η_{FP}) is the efficiency of the feed pump, (P_{FP}) is the power of the feed pump (kW), (η_{VM}) is the efficiency of the vibration motor in case of module vibration, and (P_{VM}) is the power of the vibration motor in case of module vibration (kW).

In order to provide accurate results, it is essential to consider changes in the active surface area, which significantly impacts calculations under varying test conditions. It is crucial to specify the filtration portion of the membrane surface area in question. When a spacer was integrated into the module, the active filter surface area was reduced, which should be taken into account. Table (1) presents detailed information on the results of the surface reduction calculations. By carefully taking into account these factors, we can ensure the accuracy and reliability of our experimental and computational findings.

Table 1: Useful filter surface of the membrane under different conditions

Module channel configuration	**Active membrane surface area [m^2]**
Control (without spacer), Empty membrane module channel	0.05030
Star-shaped spacer filled module channel	0.04888
Column-shaped herringbone spacer filled module channel	0.04715
Module vibration (without spacer), Empty membrane module channel	0.05030

RESULTS AND DISCUSSION

Permeate flux results

Specific permeate fluxes

The permeate flow rate through an ultrafiltration membrane, considered as a key filtration and critical parameter that determines the filtration efficiency. Quantification of the specific flux (J_{SP}) using equation 2 was performed during laboratory ultrafiltration experiments to assess one of the important performances of the laboratory ultrafiltration experiments. Figure 4 presents the time-dependent variations in specific fluxes and their stabilizations. Results show that control ultrafiltration had the lower flux values, and the spacer integration into the module could result in higher flux values with the following order: star spacer, rev column spacer, and column spacer. The membrane module vibration even had higher flux values with higher flux enhancement ratios.

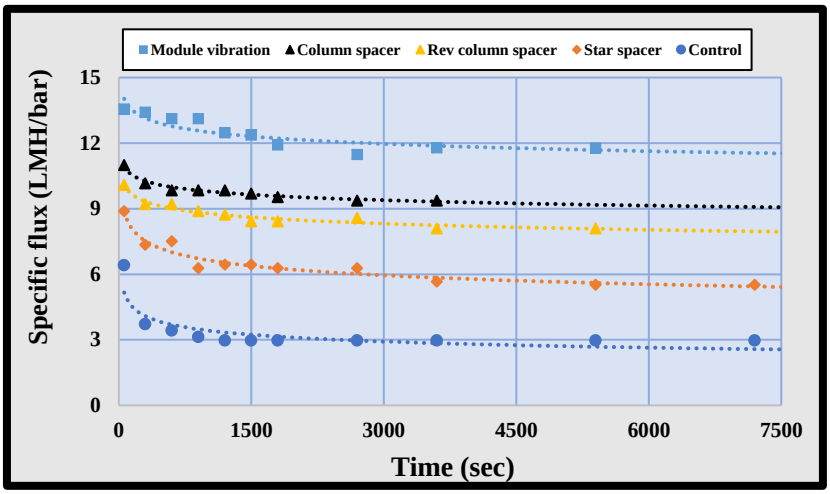

Figure 4. Permeate specific flux profiles versus ultrafiltration time. (50 kDa PES UF membrane; T=25±1°C; q_{VREC}=15.142 LPM; TMP=0.8MPa.)

Average and constant permeate fluxes

Based on the experimental results, the average and constant flux were calculated and presented in Figures 5A and 6A, respectively. The observed flux changes show significant variations between the experimental procedures tested. To emphasize the flux enhancement tendencies, their improvement ratios were demonstrated in Figures 5B and 6B. Figure 5B indicates that the integration of star spacer, rev column spacer, and column spacer into the membrane module resulted in average flux improvements of 92%, 157%, and 189%, respectively, compared to an empty membrane module channel. Figure 6B demonstrates that the integration of star spacer, rev column spacer, and column spacer led to constant flux improvements of 127%, 250%, and 300%, respectively, compared to an empty membrane module channel. Notably, vibration produced the most significant flux enhancement, as demonstrated in Figure 5B and Figure 6B, with the average permeate flux increasing by approximately 266%, and the constant flux by 409%, compared to an empty membrane module channel without vibration. These results indicate that module vibration has the most significant positive impact on permeate fluxes. Nevertheless, it is noteworthy that the column spacer alone can produce a flux improvement approaching that observed with vibration.

The utilization of the column spacer generated hydrodynamic conditions that effectively enhanced the shear rate at the membrane surface. Consequently, this increase in shear rate contributed to an augmented flow rate through the membrane. It is noteworthy that the arrangement of the column spacer in alignment with the flow direction resulted in a streamlined hydrodynamic motion. As a result, the column spacer exhibited superior flow rate

outcomes compared to the situation where the column spacer was positioned in the opposite direction (Rev column).

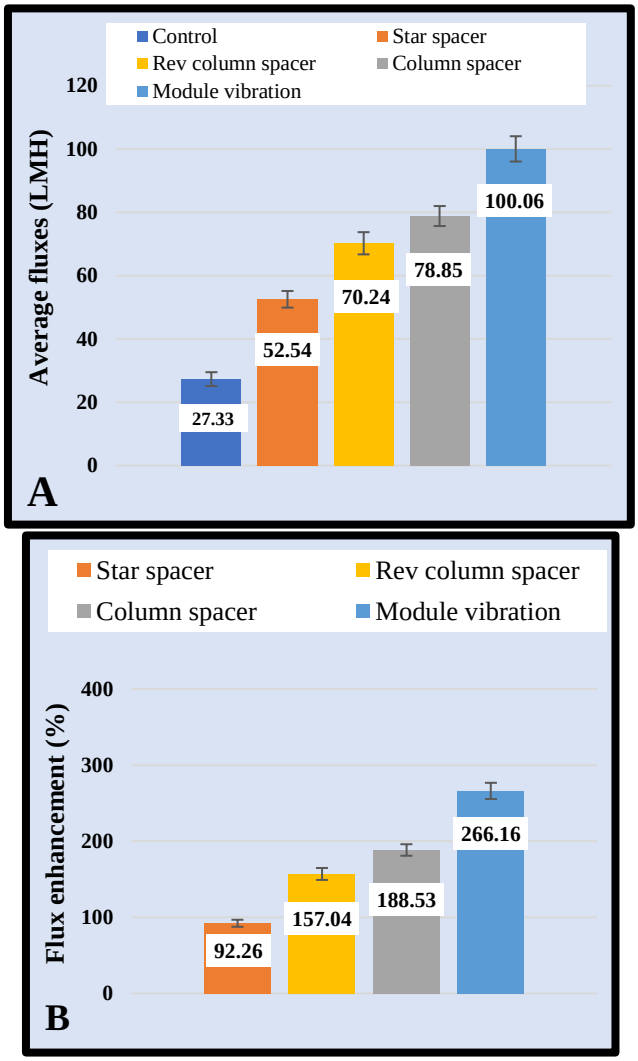

Figure 5. Effect of module-integrated 3D printed spacers and module vibration on (A) average fluxes (B) on average flux enhancement. (50 kDa PES UF membrane; T=25±1°C; q_{VREC}=15.142 LPM; TMP=0.8MPa.)

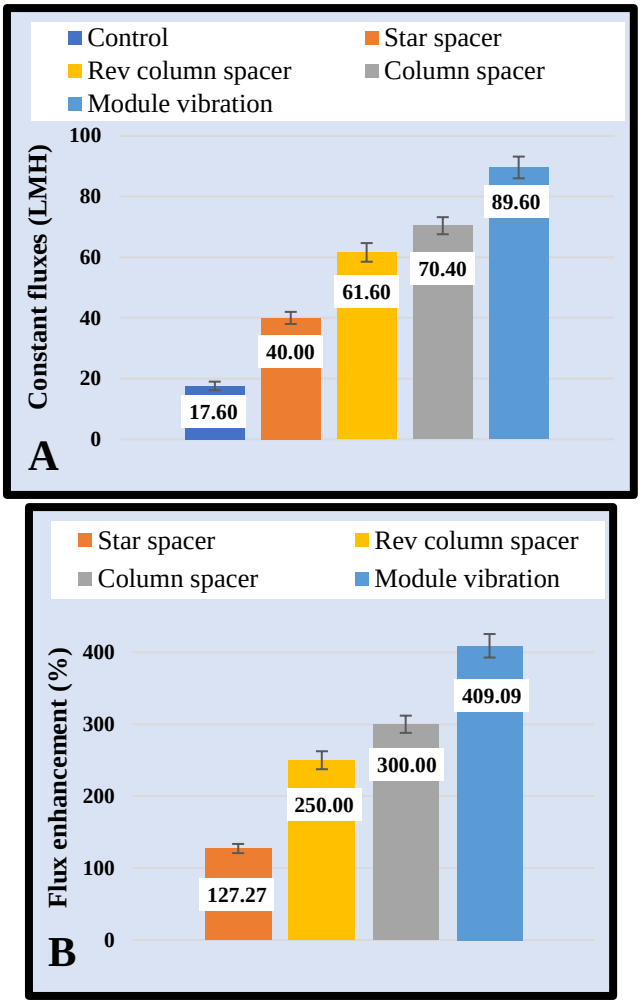

Figure 6. Effect of module-integrated 3D printed spacers and module vibration on (A) constant fluxes (B) on constant flux enhancement. (50 kDa PES UF membrane; T=25±1°C; q_{VREC}=15.142 LPM; TMP=0.8MPa.)

Volume reduction ratio results

Figure 7 depicts the volume reduction ratio (VRR) as a function of the ultrafiltration experiments time. The results show that the volume reduction ratio of two can only be attained when the module vibration is employed, and this is achieved in a relatively short period of less than one hour. With module-integrated spacers, the VRR is around 1.75, which is comparatively higher than the control value of 1.29. These results indicate that module vibration is an effective method for achieving a VRR of 2.0 in a short period. However, the use of module-integrated spacers can also lead to significantly higher VRR, albeit at a slower rate.

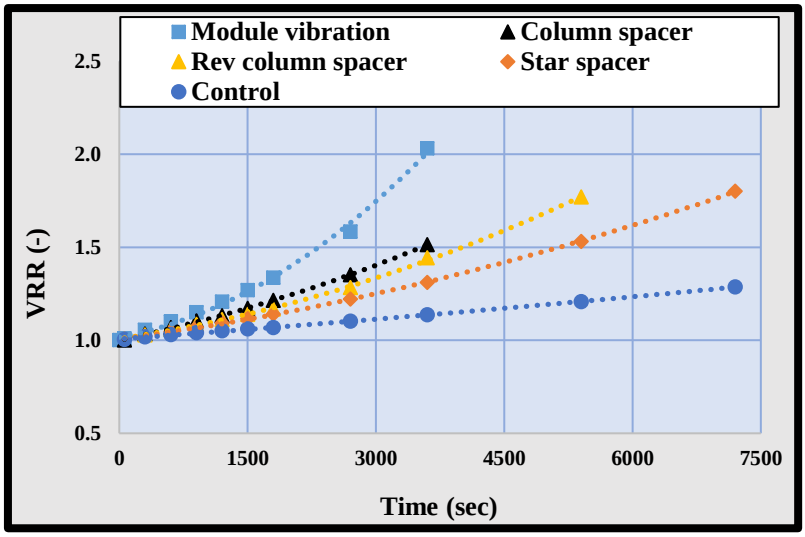

Figure 7. Volume reduction ration profiles versus ultrafiltration time.

Membrane retention analysis

Ultrafiltration retention analysis was conducted to determine the retention of various parameters by the membranes. Using equation 4, the retention can be calculated from the concentration values of feed and permeate. The retention of ions was found to be solely dependent on membrane pore sizes, with physical interference from spacers or module vibration having negligible effects. The average retention of conductivity was 10.9%. The ultrafiltration membrane also exhibited a high retention of suspended solids, with an average turbidity retention of 99.9%. The maximum difference in organic matter retention was 4.01%, with the control having the highest retention at 60.88% and the lowest retention observed with the rev column spacer integration at 56.87%, as shown in Figure 8. The slight differences in results observed can be attributed to instrument error. The results indicate that ultrafiltration membranes can effectively remove suspended solids and organic matter from the samples.

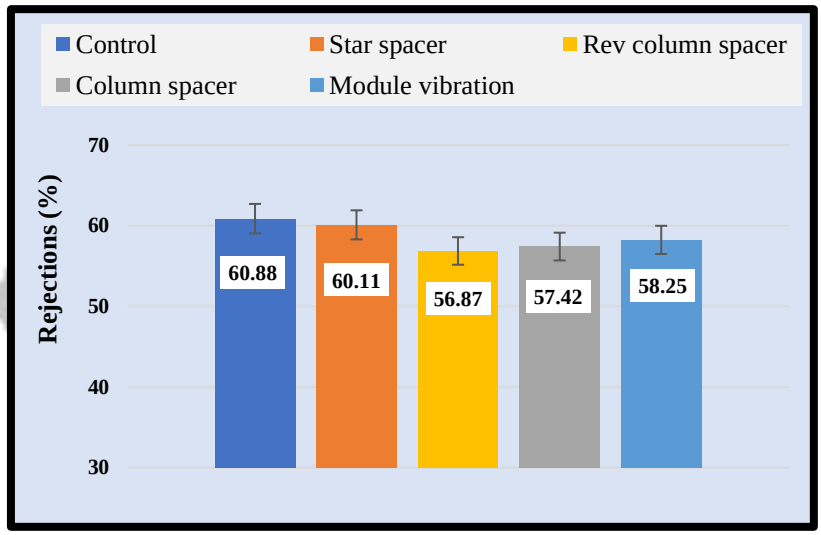

Figure 8. Organic matter membrane rejections based on Chemical Oxygen Demand (COD).

Membrane resistances

Membrane resistance is an important parameter affecting the performance of membrane filtration systems. In this study, the total resistance (R_{total}), membrane resistance (R_{membr}), reversible membrane fouling resistance (R_{rev}), and irreversible membrane resistance (R_{irrev}) were calculated using equations 5-8 and shown in Figure 9. The relative distribution of the degree of occlusion revealed that a decrease in the highly influencing reversible resistance value resulted in the most significant changes (Figure 10). Control tests showed that the specific resistance of the membrane and the degree of irreversible occlusion were similar to other tests, indicating that

only the reversible resistance served as an indicator of the difference between the different configurations. Our results show that module-integrated spacers and module vibration can significantly decrease the total and reversible resistance values. Specifically, the star spacer, rev column spacer, and column spacer module-integration individually resulted in 61.8%, 73.3%, and 74.8% total resistance reduction, and 70.7%, 82.6%, and 85.4% reversible resistance reduction. Moreover, module vibration led to a significant 78.6% total resistance reduction and 87.8% reversible resistance reduction.

Our results suggest that reversible resistance is the primary factor affecting resistance changes during ultrafiltration. The module-integrated spacers can effectively remove the polarization layer formed on the membrane surface during ultrafiltration experiments. The use of spacers in the flow direction and transmission of vibrations were found to be effective approaches for reducing the polarization layer through constant shearing at the specified frequency. These results demonstrate the potential of these methods to improve the performance and extend the lifespan of membrane filtration systems.

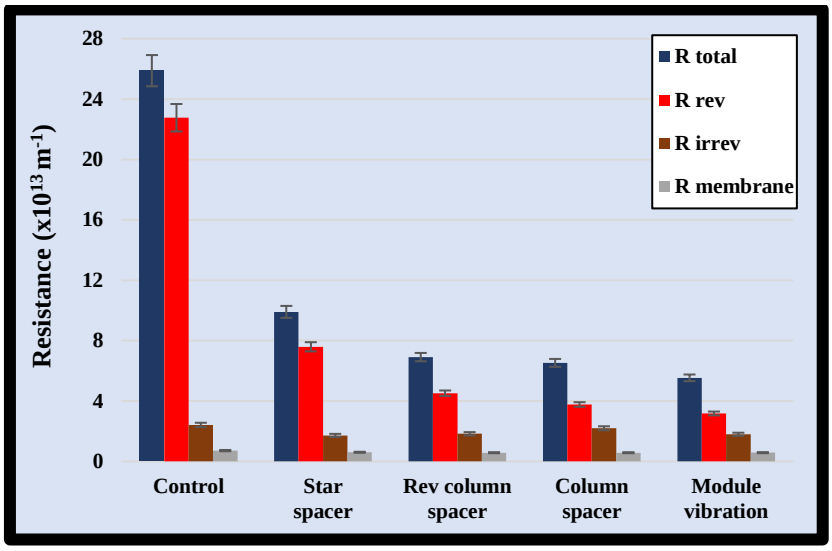

Figure 9. Effect of module-integrated 3D printed spacers and module vibration on resistances.

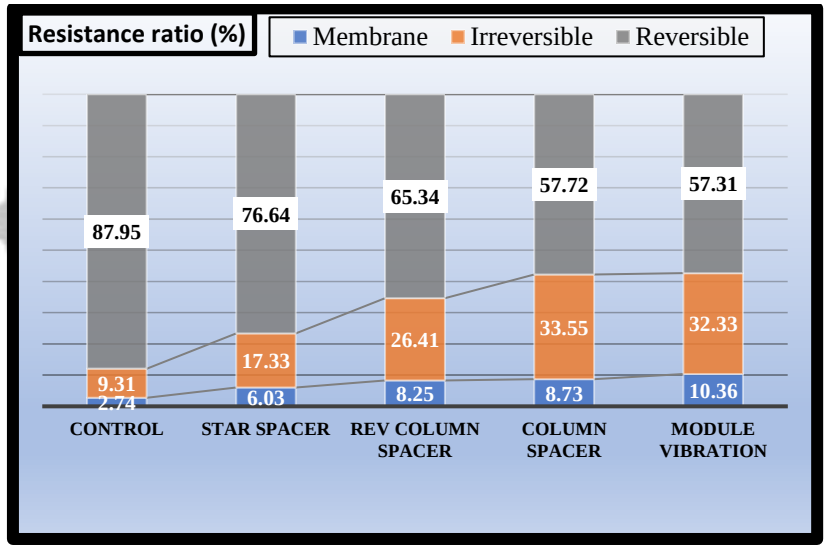

Figure 10. Effect of module-integrated 3D printed spacers and module vibration on percentage resistance ratio.

Specific energy consumption

Energy demand is an essential indicator of efficiency in processes involving machines, such as membrane separation. To maintain the TMP during membrane filtration, the feed pump must generate an appropriate volume flow, and power consumption for any motors generating module vibrations must be considered. The power requirements of the filtration process are primarily determined by the feed pump. A graphical representation of

specific energy consumption, calculated with equation 10, as a function of the VRR, is presented in Figure 11. The results indicate that the VRR provides only partial information about the amount of permeate produced. During the initial stage of ultrafiltration experiments, there is a significant change in specific energy consumption, mainly driven by flux and membrane fouling. Once the filtrate reaches a critical flow rate, the process energy consumption stabilizes. These findings are applicable to the control experiment. The experiments with module-integrated spacers and even the module vibration led to notably different, lower energy consumption results. In such cases, the average energy consumption was significantly lower, as depicted in Figure 12.

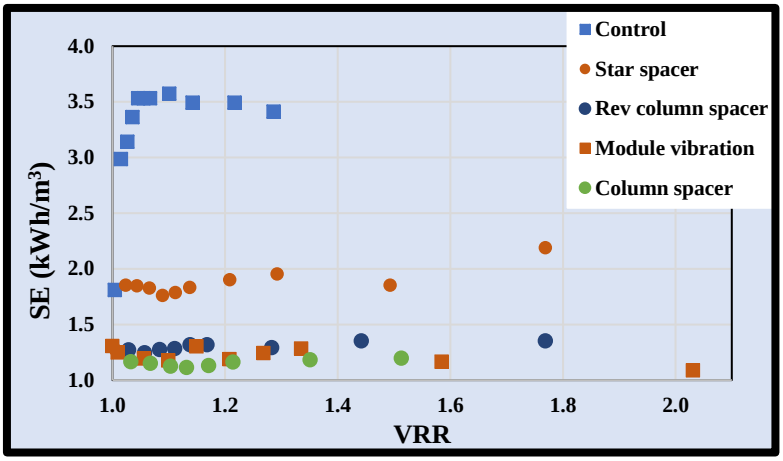

Figure 11. Effect of module-integrated 3D printed spacers and module vibration on specific energy consumption profile during ultrafiltration experiments.

Inclusion of a star spacer could reduce the specific energy consumption by almost half (45.49%) compared to the control empty channel case. The use of column spacers also resulted in a significant decrease in energy consumption in both flow directions for module integration (59.92% and 61.17%, respectively). Although the application of module vibration requires the installation of a vibration motor, it showed the greatest reduction (62.44%) in energy consumption compared to the control empty membrane module channel configuration without vibration.

Based on these data, it can be concluded that 3D printed spacer module-integration could show almost the same efficiency in terms of energy consumption as the best module vibration experiment.

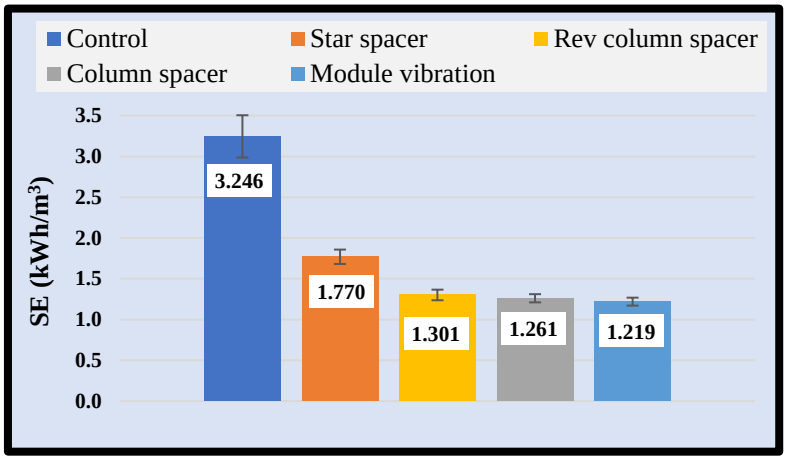

Figure 12. Effect of module-integrated 3D printed spacers and module vibration on average specific energy consumption.

CONCLUSION

In this study, the performances of an ultrafiltration membrane were evaluated by incorporating two different module-integrated 3D printed spacers into a VSEP L-mode device and module vibration. The permeate fluxes, membrane resistances, and specific energy consumption were investigated. The results show that the module-integrated spacers and vibration can significantly enhance the permeate fluxes. In particular, the column spacer outperformed the rev column spacer and star spacer regarding flux enhancement and resistance decreases. Module vibration produced the most significant flux enhancement, and the column spacer alone can also produce a flux

improvement approaching that observed with vibration. Membrane retention analysis revealed that the ultrafiltration membrane effectively removed suspended solids and about 60% of the organic matter from the raw dairy wastewater without large and significant variations. Membrane resistances were also investigated, and the results indicate that module-integrated spacers and module vibration can significantly decrease the total and reversible resistance values. Our results indicate that the membrane module vibration resulted significantly better performance than module spacers integration, but its operation means other environmental and operational difficulties in the technology.

These findings demonstrate that incorporating spacers and module vibration can improve the filtration efficiency of the ultrafiltration membrane. In conclusion, the 3D printed spacers integration into the VSEP module could be supported elements for higher ultrafiltration efficiencies and fouling mitigation. The present study provides valuable insights into designing and optimizing ultrafiltration membranes for wastewater treatment applications.

FUNDING

This study was financed by the NKFI-FK-142414 project. Sz. Kertész is grateful for the financial support of the János Bolyai Research Scholarship of the Hungarian Academy of Sciences (BO/00576/20/4) and the New National Excellence Program of the Ministry of Human Capacities (ÚNKP-22-5-SZTE-210). We also thank the University of Szeged Open Access Fund (6195) for support.

ACKNOWLEDGMENTS

The author would like to thank Balázs Szegedi for his help in conducting the experiments, Aws N. Al-Tayawi for his significant contribution in writing of the publication, and József Richárd Lennert for his role in the design of the spacers.

DATA AVAILABILITY STATEMENT

The data that support the findings of this study are available from the corresponding author upon reasonable request.

References

Akoum, O., Jaffrin, M. Y., Ding, L. H., & Frappart, M. (2004). Treatment of dairy process waters using a vibrating filtration system and NF and RO membranes. *Journal of Membrane Science*, *235*(1–2), 111–122.

Ali, S. M., Qamar, A., Kerdi, S., Phuntsho, S., Vrouwenvelder, J. S., Ghaffour, N., & Shon, H. K. (2019). Energy efficient 3D printed column type feed spacer for membrane filtration. *Water Research*, *164*, 114961.

Al-Shimmery, A., Mazinani, S., Ji, J., Chew, Y. M. J., & Mattia, D. (2019). 3D printed composite membranes with enhanced anti-fouling behaviour. *Journal of Membrane Science*, *574*, 76–85.

Andrade, L. H., Mendes, F. D. S., Espindola, J. C., & Amaral, M. C. S. (2014). Nanofiltration as tertiary treatment for the reuse of dairy wastewater treated by membrane bioreactor. *Separation and Purification Technology*, *126*, 21–29.

Aslam, M., Wicaksana, F., Farid, M., Wong, A., & Krantz, W. B. (2022). Mitigation of membrane fouling by whey protein via water hammer. *Journal of Membrane Science*, *642*, 119967.

Baitalow, K., Wypysek, D., Leuthold, M., Weisshaar, S., Lölsberg, J., & Wessling, M. (2021). A mini-module with built-in spacers for high-throughput ultrafiltration. *Journal of Membrane Science*, *637*, 119602.

Bhuvaneshwari, S., Majeed, F., Jose, E., & Mohan, A. (2022). Different treatment methodologies and reactors employed for dairy effluent treatment-A review. *Journal of Water Process Engineering*, *46*, 102622.

Bortoluzzi, A. C., Faitão, J. A., Di Luccio, M., Dallago, R. M., Steffens, J., Zabot, G. L., & Tres, M. V. (2017). Dairy wastewater treatment using integrated membrane systems. *Journal of Environmental Chemical Engineering*, *5*(5), 4819–4827.

Frappart, M., Akoum, O., Ding, L. H., & Jaffrin, M. Y. (2006). Treatment of dairy process waters modelled by diluted milk using dynamic nanofiltration with a rotating disk module. *Journal of Membrane Science*, *282*(1–2), 465–472.

Fritzmann, C., Wiese, M., Melin, T., & Wessling, M. (2014). Helically microstructured spacers improve mass transfer and fractionation selectivity in ultrafiltration. *Journal of Membrane Science*, *463*, 41–48.

Galvão, D. F. (2018). Membrane technology and water reuse in a dairy industry. *Technological Approaches for Novel Applications in Dairy Processing*, *163*.

Gáspár, I., & Neczpál, R. (2020). Testing of 3D Printed Turbulence Promoters for Membrane Filtration. *Periodica Polytechnica Chemical Engineering*, *64*(3), 371–376.

Guo, W., Ngo, H.-H., & Li, J. (2012). A mini-review on membrane fouling. *Bioresource Technology*, *122*, 27–34.

Khalil, A., Ahmed, F. E., & Hilal, N. (2021). The emerging role of 3D printing in water desalination. *Science of The Total Environment*, *790*, 148238.

Koo, J. W., Ho, J. S., An, J., Zhang, Y., Chua, C. K., & Chong, T. H. (2021). A review on spacers and membranes: Conventional or hybrid additive manufacturing? *Water Research*, *188*, 116497.

Kumar, S., Gupta, N., & Pakshirajan, K. (2015). Simultaneous lipid production and dairy wastewater treatment using Rhodococcus opacus in a batch bioreactor for potential biodiesel application. *Journal of Environmental Chemical Engineering*, *3*(3), 1630–1636.

Labbé, J. I., Ramos-Suárez, J. L., Hernández-Pérez, A., Baeza, A., & Hansen, F. (2017). Microalgae growth in polluted effluents from the dairy industry for biomass production and phytoremediation. *Journal of Environmental Chemical Engineering*, *5*(1), 635–643.

Ng, V. H., Koo, C. H., Chong, W. C., & Tey, J. Y. (2021). Progress of 3D printed feed spacers for membrane filtration. *Materials Today: Proceedings*, *46*, 2070–2077.

Nqombolo, A., Mpupa, A., Moutloali, R. M., & Nomngongo, P. N. (2018). Wastewater treatment using membrane technology. *Wastewater and Water Quality*, *29*, 30–40.

Park, S., Dal Jeong, Y., Lee, J. H., Kim, J., Jeong, K., & Cho, K. H. (2021). 3D printed honeycomb-shaped feed channel spacer for membrane fouling mitigation in nanofiltration. *Journal of Membrane Science*, *620*, 118665.

Reig, M., Vecino, X., & Cortina, J. L. (2021). Use of membrane technologies in dairy industry: An overview. *Foods*, *10*(11), 2768.

Schwinge, J., Wiley, D. E., Fane, A. G., & Guenther, R. (2000). Characterization of a zigzag spacer for ultrafiltration. *Journal of Membrane Science*, *172*(1–2), 19–31.

Shi, W., & Benjamin, M. M. (2009). Fouling of RO membranes in a vibratory shear enhanced filtration process (VSEP) system. *Journal of Membrane Science*, *331*(1–2), 11–20.

Sreedhar, N., Mavukkandy, M. O., Aminabhavi, T. M., Hong, S., & Arafat, H. A. (2022). Fouling mechanisms in ultrafiltration under constant flux: Effect of feed spacer design. *Chemical Engineering Journal*, *446*, 136563.

Sreedhar, N., Thomas, N., Al-Ketan, O., Rowshan, R., Hernandez, H., Al-Rub, R. K. A., & Arafat, H. A. (2018). 3D printed feed spacers based on triply periodic minimal surfaces for flux enhancement and biofouling mitigation in RO and UF. *Desalination*, *425*, 12–21.

Szerencsés, S. G., Beszédes, S., László, Z., Veréb, G., Szegedi, B., H Horváth, Z., Hodúr, C., Rákhely, G., & Kertész, S. (2021). Effect of vibration on the efficiency of ultrafiltration. *Analecta Technica Szegedinensia*, *15*(1), 37–44.

Tanudjaja, H. J., Anantharaman, A., Ng, A. Q. Q., Ma, Y., Tanis-Kanbur, M. B., Zydney, A. L., & Chew, J. W. (2022). A review of membrane fouling by proteins in ultrafiltration and microfiltration. *Journal of Water Process Engineering*, *50*, 103294.

Thomas, N., Sreedhar, N., Al-Ketan, O., Rowshan, R., Al-Rub, R. K. A., & Arafat, H. (2019). 3D printed spacers based on TPMS architectures for scaling control in membrane distillation. *Journal of Membrane Science*, *581*, 38–49.

Tsai, H.-Y., Huang, A., Luo, Y.-L., Hsu, T.-Y., Chen, C.-H., Hwang, K.-J., Ho, C.-D., & Tung, K.-L. (2019). 3D printing design of turbulence promoters in a cross-flow microfiltration system for fine particles removal. *Journal of Membrane Science*, *573*, 647–656. https://doi.org/10.1016/j.memsci.2018.11.081

Van Dang, B., Charlton, A. J., Li, Q., Kim, Y. C., Taylor, R. A., Le-Clech, P., & Barber, T. (2021). Can 3D-printed spacers improve filtration at the microscale? *Separation and Purification Technology*, *256*, 117776.

Yanar, N., Son, M., Yang, E., Kim, Y., Park, H., Nam, S.-E., & Choi, H. (2018). Investigation of the performance behavior of a forward osmosis membrane system using various feed spacer materials fabricated by 3D printing technique. *Chemosphere*, *202*, 708–715.

Graphical Abstract